Crystal structure of a new high-pressure polymorph of topaz-OH

MASAMI KANZAKI*

Institute for Study of the Earth's Interior, Okayama University, Misasa, Tottori 682-0193, Japan

ABSTRACT

A new high-pressure form of topaz-OH (denoted here topaz-OH II) was obtained at 14 GPa and 1400 °C. The X-ray diffraction pattern of this phase can be indexed by an orthorhombic cell with $a = 4.72318(5)$, $b = 8.91480(9)$, and $c = 2.77276(3)$ Å. The lengths of a and b are similar, but c is approximately a third of that for a previously reported topaz-OH (denoted topaz-OH I). The structural formula of topaz-OH II can be written as $(Al_{0.68}Si_{0.32})(O_{0.66}(OH)_{0.34})_2$, suggesting significant cation disorder in the structure. The crystal structure of topaz-OH II is solved using powder synchrotron X-ray diffraction data, and refined with constraints provided by a separate multi-nuclear NMR study. The structure has similarities with topaz-OH I and diaspore (α-AlOOH) structures, having partially occupied double edge-shared octahedral chains, and 2×1 tunnels with partially occupied tetrahedral and octahedral sites.

Keywords: Crystal structure, high-pressure studies, phase transition, order-disorder

INTRODUCTION

Topaz-OH [$Al_2SiO_4(OH)_2$], the OH end-member of the topaz solid-solution series, was discovered at pressures 5.5–10 GPa and 700–1000 °C (Wunder et al. 1993). Subsequent phase equilibrium studies revealed that topaz-OH is stable to 13 GPa and temperatures up to 1500 °C, beyond which topaz-OH breaks down to kyanite (Al_2SiO_5) plus fluid at higher temperature, and to phase Egg ($AlSiO_3OH$)-containing assemblages at higher pressure (Schmidt et al. 1998; Ono 1999).

The crystal structure of topaz-OH has been refined in space group *Pbnm* from single-crystal X-ray diffraction (XRD) obtained at 10 GPa and 1000 °C by Wunder et al. (1993). Northrup et al. (1994) also conducted single-crystal XRD of topaz-OH synthesized at the same *P-T* conditions, and revealed that the proton is located in two non-equivalent, half-occupied sites. Later, Chen et al. (2005) studied a topaz-OD sample synthesized at 1023 K and 7.5 GPa by neutron powder diffraction, and confirmed the conclusions of the previous studies. The latter two studies suggested the possibility of lower symmetry (*Pbn*2_1) by long-range order of the proton positions, although it was not confirmed. The possibility of *Pbn*2_1 at room temperature was supported by ab-initio calculations and infrared spectroscopic study (Churakov and Wunder 2004; Watenphul and Wunder 2010). In all these structural studies, the samples were synthesized at pressures below 10 GPa and temperatures below 1000 °C, and the cation distributions except the proton were shown to be fully ordered. This established phase is referred as "topaz-OH I" in this paper.

Recently, we have applied multi-nuclear (^1H, ^{29}Si, ^{27}Al) nuclear magnetic resonance (NMR) and Raman spectroscopy to phase Egg ($AlSiO_3OH$) and other phases in the system Al_2O_3-SiO_2-H_2O (Xue et al. 2006). In the course of this study, we discovered the existence of a new high-pressure polymorph of topaz-OH (Kanzaki et al. 2006). The stability of the phase

has been studied using in situ high-pressure X-ray diffraction (Kanzaki unpublished) and found to be stable at 13–14 GPa and 1300–1500 °C, located at the high-pressure and high-temperature corner of the topaz-OH stability field estimated (Schmidt et al. 1998; Ono 1999). Here we report the crystal structure of this phase (topaz-OH II hereafter) solved using powder synchrotron X-ray diffraction data. A combined multi-nuclear NMR and Raman study of both phase I and II is reported in a separate paper (Xue et al. 2010).

EXPERIMENTAL METHODS

Sample synthesis

The topaz-OH II sample used for the present study was synthesized using a Kawai-type double stage multi-anvil system with a DIA-type guide block driven by a 1500 ton press (SPEED1500) installed at the beamline BL04B1 of SPring-8 (Utsumi et al. 1998). The starting material was a mixture of dried reagent-grade SiO_2, Al_2O_3, and $Al(OH)_3$ with a nominal $Al_2SiO_4(OH)_2$ composition, and was put into a $Pd_{75}Ag_{25}$ capsule (1.40/1.25 mm in o.d./i.d.). A 14 mm edge-length Cr-doped MgO octahedral cell assembly with a tube heater (made of hBN plus TiB_2) was employed. A thermocouple ($W_{97}Re_3$-$W_{75}Re_{25}$) was broken during compression, and thus temperature was estimated from applied electric power (with an uncertainty of ±50 °C). The pressure cell is identical to that used for in situ high-pressure and high-temperature X-ray diffraction study of topaz-OH phase, in which gold powder was used as a pressure standard (Kanzaki unpublished). However, the present synthesis experiment was conducted without in situ X-ray diffraction. Therefore, to estimate the pressure, a pressure calibration curve against press load was constructed based on 10 in situ X-ray runs. The pressure reported here is based on that curve, and the estimation error is <1 GPa.

The sample was kept at 14 GPa and 1400 °C for an hour, and then quenched by cutting off the heating power. The recovered sample (K071126) was checked by Raman spectroscopy, and was confirmed to consist of topaz-OH II with a minor stishovite phase. This sample was further characterized in detail by NMR (Xue et al. 2010). The composition of topaz-OH II determined by an electron microprobe is 58.54(0.86) wt% Al_2O_3, 31.72(0.56) wt% SiO_2, and 90.26(1.17) wt% total (20 points average). Details of the analyses including topaz-OH I and II synthesized at different *P-T* conditions are reported in Xue et al. (2010). The Si/Al ratio is calculated as 0.46(1), lower than that of the ideal composition (1/2), which explains the existence of minor stishovite in the recovered sample. If all remaining Si is used to form stishovite, 3.0(0.8) wt% of stishovite is expected from the observed Si/Al ratio and nominal bulk composition. This compares well with 2.6 wt% of stishovite

* E-mail: mkanzaki@misasa.okayama-u.ac.jp

obtained by a quantitative analysis of the Rietveld refinement (see below). The chemical formula is calculated as $Al_{2.05}Si_{0.95}O_{3.95}(OH)_{2.05}$, assuming total six O atoms and Al+H substitution for Si. Similar Si/Al ratio is also reported for topaz-OH I synthesized at the P-T conditions near the I/II phase boundary (Xue et al. 2010). Therefore, topaz-OH II reported here should be a polymorph of topaz-OH I, not an independent phase with a different Si/Al ratio.

X-ray diffraction

Powder X-ray diffraction data at ambient conditions were obtained at beam-line BL19B2 of SPring-8. A large Debye-Scherrer camera with an imaging plate detector was used. This camera is identical to the one in BL02B2, and details of the camera are described in Nishibori et al. (2001). The camera covers a 2θ range from 0 to 80° with angle resolution of 0.01°. After the NMR study (Xue et al. 2010), about half of the sample was ground in an agate mortar, and a portion <1 mg was loaded into a borosilicate glass capillary tube with 0.3 mm o.d. The capillary tube was rotated at 1 rpm during the measurement to reduce the effects of preferred orientation. The exposure time for the measurement was 10 min. A strip of 2D pattern recorded on the imaging plate was converted into conventional 1D pattern using ImageJ software (Abramoff et al. 2004) with a macro program provided by the beamline. To determine the wavelength of the X-ray beam used, a diffraction pattern of the NIST standard CeO_2 was also obtained using the identical setup. The X-ray wavelength was determined to be 1.00036 Å. The powder pattern was indexed using TREOR90 (Werner et al. 1985). The initial structure of topaz-OH II was modeled using a real-space searching program, FOX (Favre-Nicolin and Černý 2002). FOX randomly moves and rotates atoms and user-defined polyhedra or molecules in real space and calculates the powder diffraction pattern, and then compares it with the observed one. By using parallel tempering, FOX searches the best structure that reproduces the observed diffraction pattern. In the present starting configuration, we employed one AlO_6 octahedron and an additional cation site. The structure obtained by FOX was then refined with the Rietveld refinement technique using RIETAN-FP program (Izumi and Momma 2007). For the profile function, the split pseudo-Voigt function of Toraya (1990) was used. As described below, there is significant cation site disorder in the structure. For the Rietveld refinement, two minor phases, stishovite and $Pd_{75}Ag_{25}$ alloy (contaminated from the capsule) were also included. To constrain site occupancies, information obtained by NMR for the same sample (Xue et al. 2010) was used. Because the structure is significantly disordered, the contribution of the proton was ignored in the refinement.

RESULTS AND DISCUSSION

Lattice parameters

The powder diffraction pattern of topaz-OH II is shown in Figure 1. The major diffraction peaks of topaz-OH II are listed in Table 1 along with those of topaz-OH I from Wunder et al. (1993). The peak positions of topaz-OH II are similar to those of topaz-OH I; however corresponding peaks of $l \neq 3n$ (of topaz-OH I) are all missing in topaz-OH II. Indexing of the pattern using TREOR90 (Werner et al. 1985) gave an orthorhombic cell with $a = 4.72318(5)$, $b = 8.91480(9)$, and $c = 2.77276(3)$ Å (refined values by the Rietveld refinement). Those of topaz-OH I reported by Wunder et al. (1993) are as follows; $a = 4.724$, $b = 8.947$, and $c = 8.390$ Å. Although the lengths of a- and b-axes are similar, the c-axis in topaz-OH II is about a third of that in topaz-OH I, explaining the absence of the peaks with $l \neq 3n$ in topaz-OH II. The number of formulae in the unit cell (Z) for topaz-OH II becomes 4/3, if the nominal structural formula for topaz-OH ($Al_2SiO_4(OH)_2$) is used. To have an integer Z number (4), the nominal structural formula for topaz-OH II should be rewritten as $(Al_{2/3}Si_{1/3})(O_{2/3}OH_{1/3})_2$. Taking account of the observed Al/Si ratio, the structural formula for the present sample becomes $(Al_{0.68}Si_{0.32})(O_{0.66}(OH)_{0.34})_2$. This new formula for topaz-OH II suggests cation disorder in the structure, as was verified by NMR and Raman spectroscopy (Xue et al. 2010). The reported volumes of topaz-OH I are 355.92(3) (Wunder et al. 1993) and 354.5(2) Å³ (Northrup et al. 1994). The volume of
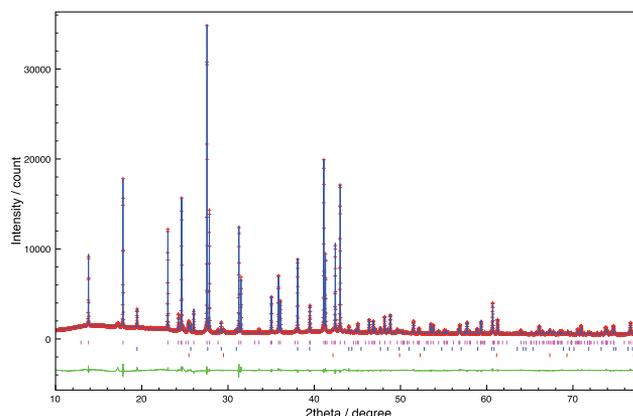

FIGURE 1. The results of Rietveld refinement. Crosses are observed data and the solid line is the calculated pattern. The line at bottom is the difference. Top, middle, and bottom vertical ticks show the peak positions of topaz-OH II, stishovite, and $Pd_{75}Ag_{25}$, respectively. A broad small peak at 17.2° is due to graphite (possibly originating from absorbed CO_2 on the starting material).

TABLE 1. Comparison of major diffraction peaks of topaz-OH I and II

Topaz-OH II (obs)			Topaz-OH I	
d_{obs}	hkl	I/I_0 (%)	d_{cal}	hkl
4.1737	110	24	4.1774	110
–	–	–	3.7395	111
3.2418	120	39	3.2482	120
–	–	–	3.0601	022
–	–	–	3.0291	121
–	–	–	2.9601	112
2.5153	130	34	2.5219	130
–	–	–	2.4151	131
2.3912	101	5	2.4065	103
2.3545	021	47	2.3714	023
2.1072	121	100	2.1194	123
2.0868	220	42	2.0887	220
–	–	–	1.8745	114
1.8630	131	36	1.8729	133
1.8489	230	18	1.8516	230
–	–	–	1.6939	232
1.6674	221	14	1.6734	223
1.6304	141	21	1.6384	143
1.5383	231	23	1.5439	233
1.4846	320	11	1.4853	320
1.4294	151	65	1.4360	153
1.4230	250	13	1.4263	250
1.3864	002	35	1.3983	006
1.3691	301	62	1.3721	303

* d-spacings of major reflections of topaz-OH I calculated using reported structure parameters by Wunder et al. (1993).

topaz-OH II [350.251(7) Å³, tripled to compare with topaz-OH I] is smaller than those of topaz-OH I by 1.1~1.6%, supporting our observation that topaz-OH II is a higher pressure form than topaz-OH I.

Structure analysis

Systematic absences are consistent with space group *Pbnm*, the same as topaz-OH I. Structural similarity between topaz-OH II and diaspore (α-AlOOH) was noticed. The space group and cell parameters are comparable to those of diaspore. The cell parameters for diaspore are given here for comparison (Hill 1979); *Pbnm*, $a = 4.4007$, $b = 9.4253$, and $c = 2.8452$ Å. The structure of diaspore viewed from c-direction is shown in Figure 2a. We first modeled the structure by putting one octa-

hedral Al atom in the 4c Wyckoff position of the *Pbnm* cell. A diaspore-like structure is readily obtained by FOX with R_{wp} = 23.6%. Here we denote this octahedral site of the structure as Oc1 site. The differential Fourier map shows a peak in a vacant tetrahedral site, which is located in the 2 × 1 octahedral tunnel of the diaspore-like structure (see Fig. 2a). By putting a Si atom in this tetrahedral site (denoted as the T site hereafter) with an occupancy of 1/3, and reducing occupancy of the Oc1 site to 2/3, the structure refines further by FOX to R_{wp} = 17.7%, and the structure obtained is shown in Figure 2b. The differential Fourier map now shows a small peak in a vacant octahedral site in the tunnel. By putting a Si atom in this octahedral site (denoted here as Oc2 site) with an occupancy unfixed, R_{wp} dropped further to 13.1%. No additional peaks could be clearly resolved in the differential Fourier map at this stage. Using this structure as the initial structural parameters, the Rietveld refinement was conducted with the RIETAN-FP program (Izumi and Momma 2007). To place constraints on the occupancy of cation sites, the information obtained by a separate NMR spectroscopic study of the same sample was used (Xue et al. 2010). The ^{29}Si MAS NMR study revealed that 63(1)% of total Si is in tetrahedral, whereas the remaining 37% is in octahedral coordination. ^{27}Al 3Q MAS NMR showed that 2.2(1)% of total Al is in tetrahedral coordination. From the NMR, the T site is occupied by 0.198 Si and 0.015 Al. It was not possible to constrain occupancies of the remaining Al and Si in Oc1 and Oc2 octahedral sites. Therefore, random Al/Si distribution for two octahedral sites was assumed (i.e., $Al_{0.851}Si_{0.149}$), with the total occupancy of the octahedral sites (Oc1 and Oc2) fixed at 0.787 during the refinement. No partial occupancies for oxygen sites are assumed. If the Oc2 site was omitted in the refinement, the R values increased significantly, which supports real occupancy of the Oc2 site. The isotropic atomic displacement parameter for Oc2 became improbably small, when it was not fixed. Therefore, this parameter was constrained to be the same as that of the T site. The refinement converged to R_{wp} = 4.22% and S = 1.36. Bragg R values for topaz-OH II are $R_B(R_I)$ = 4.52 and R_F = 4.16%.

The results of the Rietveld refinement are shown in Figure 1. The structural parameters obtained are listed in Table 2, and the crystal structure is shown Figure 2c. The isotropic atomic displacement factors for all atoms are a few times larger than com-
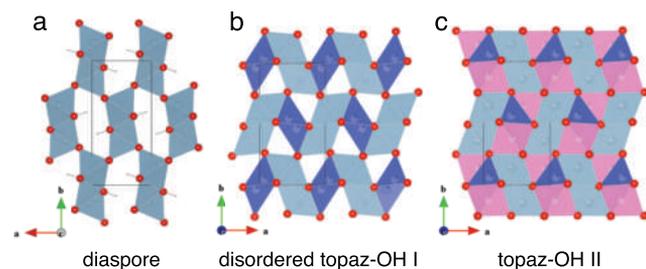
monly obtained values. This could be due to extensive disorder and partial occupancies of cations in all sites in the structure.

Structure of topaz-OH II

The structure of topaz-OH II is closely related to diaspore and topaz-OH I structures as explained below. The structures of all three phases are based on hexagonal close-packing (HCP) arrangement of O atoms, and structural differences between the phases are due to cation distributions on octahedral and tetrahedral interstices in the HCP. In the structure of diaspore, half of the available octahedral interstices are occupied by Al (Hill 1979). Each Al octahedron shares four edges with other octahedra, and forms a double octahedral chain running parallel to the *c*-axis (Fig. 2a). Each double octahedral chain shares corners with other chains, and those chains form 2 × 1 octahedral tunnels. In the structure of topaz-OH I, there are one octahedral Al and one tetrahedral Si sites and one third of the available octahedral interstices in the HCP are occupied by Al. Each Al octahedron shares two edges with other octahedra, forming kinked single octahedral chains running in the *c*-direction. Alternatively, this chain can be obtained by removing 1/3 of the Al atoms from the double octahedral chain in diaspore. The tetrahedral Si site in topaz-OH I is located in the corresponding 2 × 1 tunnel of the diaspore structure. A vacant tetrahedral site is next to the tetrahedral Si site, and these tetrahedra form straight corner-shared tetrahedral chains running in along the *c*-axis. Only 1/3 of tetrahedral site in the chain are occupied by Si. The vacant tetrahedral site in the chain shares a face with a neighboring Al octahedron. The vacant octahedral site in the kinked chain shares a face with the occupied tetrahedral Si site. Therefore, Al and Si distributions in topaz-OH I are in an ordered arrangement, so that occupied polyhedra do not share faces. The structure of topaz-OH II (Fig. 2c) has the double octahedral chain made by Oc1, however it is not fully occupied. Therefore, the short-range structure of this chain will be similar to that of the kinked chain in topaz-OH I. The T site forms single corner-shared tetrahedral chains in the 2 × 1 tunnel, and is partially occupied. As noted above, the corresponding chain exists in the topaz-OH I, however, the Si distribution is ordered. Therefore, topaz-OH II can be regarded as a cation disordered variation of the topaz-OH I structure in the octahedral and tetrahedral chains along the *c*-axis. The corresponding disordered structure is shown in Figure 2b. The present study reveals another octahedral site (Oc2) located in the 2 × 1 tunnel. This site has no corresponding occupied octahedral site in topaz-OH I and diaspore. Ramsdellite (MnO_2) is isostructural with diaspore, and it can incorporate Li ion into the structure by reducing valence state of Mn (Li_xMnO_2). The

diaspore — disordered topaz-OH I — topaz-OH II

FIGURE 2. Structural comparison of diaspore (α-AlOOH), "disordered topaz-OH I," and topaz-OH II viewed along the *c*-axis. Light sky-blue octahedron represents Oc1 site in all three structures. The small pink sphere in the diaspore structure is the proton. Blue tetrahedra and pink octahedra represent T1 and Oc2 sites in the latter two structures, respectively. The structures are drawn by VESTA (Momma and Izumi 2008).

TABLE 2. Refined atomic parameters of topaz-OH II

Site	Atom	Occupancy	x	y	z	U (Å^2)
O1	O	1	0.5891(2)	0.2482(1)	1/4	0.0282(4)
O2	O	1	0.2365(2)	0.5098(1)	1/4	0.0334(4)
T	$Al_{0.07}Si_{0.93}$	0.213	0.5876(5)	0.4402(3)	1/4	0.0163(5)
Oc1	$Al_{0.851}Si_{0.149}$	0.705(1)	0.5812(2)	0.8587(1)	1/4	0.0213(2)
Oc2	$Al_{0.851}Si_{0.149}$	0.082†	0.579(1)	0.6298(7)	1/4	0.0163*

Notes: Lattice constants: a = 4.72318(5), b = 8.91480(9), c = 2.77276(3) Å, V = 116.750(2) Å^3, Space group: *Pbnm*, Z = 4 for $(Al_{0.68}Si_{0.32})(O_{0.66}(OH)_{0.34})_2$. R_{wp} = 4.22%, S = 1.36, R_I = 4.52%, R_F = 4.16%. All atoms are in 4c site.
* U constrained; $U_T = U_{Oc2}$.
† Total occupancy fixed; Oc1 + Oc2 = 0.787 = 1 – T.

Li ion is located in an octahedral site corresponding to the Oc2 site of topaz-OH II (Thackeray et al. 1993). The Oc1 site is fully occupied, whereas the T site is not occupied at all in this intercalated ramsdellite. The face sharing of the Li ion with the Oc1 site is possible for this phase given the smaller charge of Li ion compared to Al or Si, although significant buckling of the structure due to the face-sharing was observed with increasing Li content (Thackeray et al. 1993).

The obtained occupancies of the T, Oc1, and Oc2 sites are 0.214, 0.705, and 0.082, respectively. The occupancies of the corresponding T, Oc1, and Oc2 sites in disordered topaz-OH I calculated using the observed composition are 0.31, 0.69, and 0, respectively. Compared to disordered topaz-OH I, a third of the Si in the T site is moved to the Oc1 and Oc2 sites. The Oc2 site apparently accepts more excess cations from the T site than the Oc1 site. Formation of the Oc2 site in topaz-OH II could account for the reduced occupancy of the T site from 0.31 to 0.214, because of the possibility to share a face between Oc2 and the neighboring T sites is decreased. Only minor tetrahedral Al (0.015) was detected in the T site by ^{27}Al 3Q MAS NMR (Xue et al. 2010), thus, disordering of Si-Al between tetrahedral and octahedral sites is insignificant. Therefore, structural changes that occur on the transition from topaz-OH I to II include formation of octahedral Si and correspondingly less tetrahedral Si, extensive disordering of the cation distribution on cation sites, and resultant loss of long-range order along the *c*-axis.

Selected bond distances are shown in Table 3. The O2 is located in the center of the edge-sharing double octahedral chains, and is at the junction of three shared-edges. The O1 is at the junction of two shared edges and one shared corner. The Oc1-O2 distances are longer than those of Oc1-O1; due to repulsion of Al/Si ions in edge-shared octahedral sites, a similar trend can be also found in diaspore (Hill 1979). The average Oc1-O distance is 1.918 Å, and is close to the bond length estimated from ionic radii of octahedral Al^{3+} and O^{2-} (1.93 Å; Shannon 1976). This might suggest that the Oc1 site is mostly occupied by Al, however, partial occupancy (0.705) makes reliable estimation of Al/Si ratio from bond distance difficult. The average bond distances of Oc2-O (1.968 Å) and T-O (1.709 Å) are apparently larger than those expected from ionic radii. This can be explained by the small occupancies of cations in these sites as described above.

No structural information regarding proton sites in topaz-OH II can be obtained from the present X-ray diffraction study, although disorder of the protons is expected because ^{1}H NMR and Raman spectroscopy of topaz-OH II (Xue et al. 2010) has confirmed significant disorder on proton sites. For disordered hydrous phases, combined application of both diffraction and spectroscopy techniques is indispensable.

Finally, topaz-OH II reveals new crystal-chemical insight of cation disorder in dense hydrous phases, and a structural relation-ship between diaspore, intercalated ramsdellite and topaz-OH phases. Since topaz-OH II has an exceptionally high thermal stability (to 1500 °C), the phase could be stabilized in subducted sediments, bringing water into the mantle transition zone.

REFERENCES CITED

Abramoff, M.D., Magelhaes, P.J., and Ram, S.J. (2004) Image Processing with ImageJ. Biophotonics International, 11, 36–42.

Chen, J.R., Lager, G.A., Kunz, M., Hansen, T.C., and Ulmer, P. (2005) A Rietveld refinement using neutron powder diffraction data of a fully deuterated topaz, $Al_2SiO_4(OD)_2$. Acta Crystallographica Section E-Structure Reports Online, 61, I253–I255.

Churakov, S.V. and Wunder, B. (2004) Ab-initio calculations of the proton location in topaz-OH, $Al_2SiO_4(OH)_2$. Physics and Chemistry of Minerals, 31, 131–141.

Favre-Nicolin, V. and Černý, R. (2002) FOX, "Free objects for crystallography:" A modular approach to ab initio structure determination from powder diffraction. Journal of Applied Crystallography, 35, 734–743.

Hill, R.J. (1979) Crystal structure refinement and electron density distribution in diaspore. Physics and Chemistry of Minerals, 5, 179–200.

Izumi, F. and Momma, K. (2007) Three-dimensional visualization in powder diffraction. Solid State Phenomena, 130, 15–20.

Kanzaki, M., Xue, X., Fukui, H., and Ito, E. (2006) High-pressure form of topaz-OH: Structure and characterization by NMR and Raman. 9th General Meeting of the International Mineralogical Association (IMA), Abstract, P06-05, Kobe, Japan.

Momma, K. and Izumi, F. (2008) VESTA: a three-dimensional visualization system for electronic and structural analysis. Journal of Applied Crystallography, 41, 653–658.

Nishibori, E., Takata, M., Kato, K., Sakata, M., Kubota, Y., Aoyagi, S., Kuroiwa, Y., Yamakata, M., and Ikeda, N. (2001) The large Debye-Scherrer camera installed at SPring-8 BL02B2 for charge density studies. Nuclear Instruments and Methods in Physics Research, A 467–468, 1045–1048.

Northrup, P.A., Leinenweber, K., and Parise, J.B. (1994) The location of H in the high-pressure synthetic $Al_2SiO_4(OH)_2$ topaz analogue. American Mineralogist, 79, 401–404.

Ono, S. (1999) High temperature stability limit of phase egg, $AlSiO_3(OH)$. Contributions to Mineralogy and Petrology, 137, 83–89.

Schmidt, M.W., Finger, L.W., Angel, R.J., and Dinnebier, R.E. (1998) Synthesis, crystal structure, and phase relations of $AlSiO_3OH$, a high-pressure hydrous phase. American Mineralogist, 83, 881–888.

Shannon, R.D. (1976) Revised effective ionic radii and systematic studies of interatomic distances in halides and chalcogenides. Acta Crystallographica, A32, 751–767.

Thackeray, M.M., Rossouw, M.H., Gummow, R.J., Liles, D.C., Pearce, K., De Kock, A., David, W.I.F., and Hull, W. (1993) Ramsdellite-MnO_2 for lithium batteries: The ramsdellite to spinel transformation. Electrochimica Acta, 38, 1259–1267.

Toraya, H. (1990) Array-type universal profile function for powder pattern fitting. Journal of Applied Crystallography, 23, 485–491.

Utsumi, W., Funaloshi, K., Urakawa, S., Yamakata, M., Tsuji, K., Konishi, H., and Shimomura, O. (1998) SPring-8 beamlines for high pressure science with multi-anvil apparatus. The Review of High Pressure Science and Technology, 7, 1484–1486.

Watenphul, A. and Wunder, B. (2010) Temperature dependence of the OH-stretching frequencies in topaz-OH. Physics and Chemistry of Minerals, 37, 65–72.

Werner, P.E., Eriksson, L., and Westdahl, M. (1985) TREOR, a semi-exhaustive trial-and-error powder indexing program for all symmetries. Journal of Applied Crystallography, 18, 3.

Wunder, B., Rubie, D.C., Ross, C.R.I., Medenbach, O., Seifert, F., and Schreyer, W. (1993) Synthesis, stability and properties and of $Al_2SiO_4(OH)_2$: A fully hydrated analogue of topaz. American Mineralogist, 78, 285–297.

Xue, X.Y., Kanzaki, M., Fukui, H., Ito, E., and Hashimoto, T. (2006) Cation order and hydrogen bonding of high-pressure phases in the Al_2O_3-SiO_2-H_2O system: An NMR and Raman study. American Mineralogist, 91, 850–861.

Xue, X.Y., Kanzaki, M., and Fukui, H. (2010) Unique crystal chemistry of two polymorphs of topaz-OH: A multi-nuclear NMR and Raman study. American Mineralogist, 95, 1276–1293.

TABLE 3. Selected bond distances (Å)

Oc1-O2	1.958(1) ×2	Oc2-O2	1.939(6) ×1
Oc1-O1	1.843(1) ×1	Oc2-O2	2.057(4) ×2
Oc1-O1	1.865(1) ×2	Oc2-O1	1.933(4) ×2
Oc1-O2	2.017(1) ×1	Oc2-O1	1.890(5) ×1
T-O2	1.677(2) ×2		
T-O2	1.770(3)		
T-O1	1.712(3)		